


Transition from half-filled stripe to Néel antiferromagnetism in the t' -Hubbard model on the honeycomb lattice

Yang Shen¹ and Mingpu Qin^{1,2,*}

¹Key Laboratory of Artificial Structures and Quantum Control, School of Physics and Astronomy, Shanghai Jiao Tong University, Shanghai 200240, China

²Hefei National Laboratory, Hefei 230088, China

 (Received 23 July 2023; revised 12 December 2023; accepted 14 December 2023; published 10 January 2024)

We study the ground state of the doped Hubbard model on honeycomb lattice with both nearest (t) and next-nearest-neighbor hoppings (t') in the small doping and strongly interacting region. Previous study on the model without t' showed the ground state is a half-filled stripe. We employ density matrix renormalization group and extrapolate the results with truncation errors in the converged region. In the $t' < 0$ side, we find the half-filled stripe phase at $t' = 0$ is stable against the frustration of t' until a critical point $-0.4 < t'_c < -0.3$, beyond which the ground state switches to antiferromagnetic Néel phase with charge modulation. With further increase of t' to -0.7 , the ground state becomes paramagnetic. In the $t' > 0$ side, the half-filled stripe stretches to $t' \approx 0.7$. We do not find obvious enhancement of pairing for the range of t' studied. We study width-4 cylinders in this paper but the results for spin, charge, and pairing correlation agree qualitatively for periodic and antiperiodic boundary conditions in the half-filled stripe and antiferromagnetic Néel phases, suggesting the results are likely to be representative for true two-dimensional systems. The half-filled stripe to antiferromagnetic Néel phase transition can be realized on real materials or ultracold atom platform.

DOI: [10.1103/PhysRevB.109.024505](https://doi.org/10.1103/PhysRevB.109.024505)

I. INTRODUCTION

Understanding the physics of doped Mott insulators is crucial to reveal the microscopic mechanism of high- T_c superconductivity [1]. Hubbard model and its descendant, i.e., $t - J$ model, are the prototype models to study Mott-related physics [2–5]. With a simple form, Hubbard model can host many exotic quantum states [2–5].

Recently, progresses have been made in the study of the doped Hubbard model on the square lattice [6]. Collaboration of state-of-the-art numerical methods [7] established the filled-stripe phase in the doped Hubbard model. It was also found that the “pure” Hubbard model (with only nearest-neighbor hoppings) on square lattice does not host superconductivity in its ground state [8].

The Hubbard model on honeycomb lattice [9] has also been extensively studied, partly due to the interests in the correlation-driven metal-insulator transition and the connection to graphene [10,11]. Similar to the square lattice, honeycomb lattice is bipartite, and the half-filled Hubbard model on honeycomb lattice is also a Mott insulator with antiferromagnetic (AF) Néel order at strong interactions [11,12]. These similarities make honeycomb lattice another playground to study Mott-related physics and to explore possible mechanisms of high- T_c superconductivity. Recent calculation showed the ground state of the slightly doped Hubbard model on honeycomb lattice also has stripe order similar as the square-lattice case [13,14]. The difference between them is

that the filling of stripe on honeycomb lattice is $1/2$ [13,14]. This finding was also confirmed by followed calculations [15,16].

Given that superconductivity is absent in the pure Hubbard model on the square lattice [8], other terms need to be included in the Hamiltonian to search for the possible superconducting ground state. The simplest term is the next-nearest-neighbor hoppings t' . To account for the particle-hole asymmetry of the phase diagram of cuprates [3], a nonzero t' term is needed in the framework of single band Hubbard model. Recent calculation for the t' -Hubbard model on square lattice showed superconductivity indeed emerges with the inclusion of t' [17]. It is argued that t' frustrates the stripe phase and helps the pairs across the stripes to build coherence, so the long-range superconducting order emerges [17].

The inclusion of t' term in the Hubbard model on honeycomb lattice also frustrates the Néel order. Actually, the strong-coupling limit of the Hubbard model with t' at half-filling, i.e., $J_1 - J_2$ Heisenberg model on honeycomb lattice, has a rich phase diagram [19,20]. It was shown that there is an AF Néel phase on the small J_2 side ($J_2 \lesssim 0.2J_1$) [21,22], and a staggered valence-bond solid phase on the large J_2 side ($J_2 \gtrsim 0.4J_1$) [23,24]. In the intermediate region, the frustrated exchange melts the AF Néel state and results in competing phases including various quantum spin liquids and plaquette valence bond solid state [19,20]. Based on these results, it is natural to ask whether superconductivity can be also enhanced by t' for the Hubbard model on the honeycomb lattice.

In this paper, we systematically study the ground-state properties of the doped Hubbard model with both t and t' on honeycomb lattice in the strong interacting and slight

*qinmingpu@sjtu.edu.cn

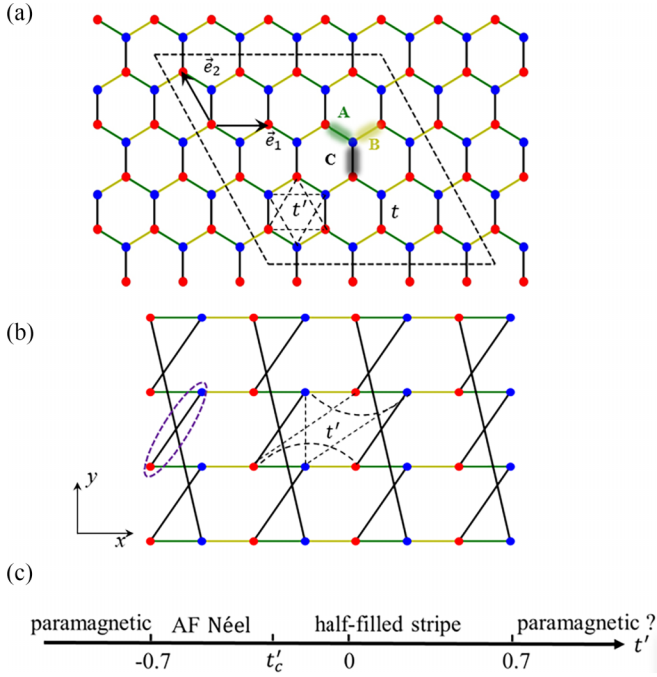


FIG. 1. (a) Sketch of the honeycomb lattice, which is rearranged into a square lattice in (b). Blue and red dots represent two inequivalent sublattices, respectively. Bonds along different directions are distinguished with colors and are labeled as A, B, and C. The two arrows in (a) are the primitive vectors of the Bravais lattice. The C bond in the dashed oval in (b) is the reference bond when calculating the pair-pair correlation function. We also vary the position of the reference C bond when calculating pair-pair correlations to analyze the boundary effect (details can be found in the Supplemental Material [18]). Black dashed lines in (a) and (b) represent the next-nearest-neighbor hopping t' on honeycomb and the corresponding square lattices, which connect sites within the same sublattices in the hexagon in (a) and corresponding plaquette in (b). Periodic/antiperiodic (open) boundary conditions are imposed for the vertical (horizontal) direction. (c) shows a phase diagram based on the DMRG results in Figs. 2 and 3, in which t'_c ($-0.4 < t'_c < -0.3$) denotes the critical point of the phase transition between half-filled stripe and AF Néel phases.

doping region. We employ density matrix renormalization group (DMRG) [25,26], which can provide accurate results for narrow cylinders [27,28]. We study the evolution of the ground state with t' in both positive and negative sides. The noninteracting dispersion can be found in the Supplemental Material [18]. At the negative t' side, we find the half-filled stripe state, previously found in the absence of t' [13,14], is stable against the frustration of t' until a critical point t'_c between -0.3 and -0.4 , at which a phase transition from half-filled stripe to AF Néel phase with charge modulation occurs. With the further increase of t' to about -0.7 , the ground state becomes paramagnetic and the charge modulation disappears. At the positive t' side, the half-filled stripe stretches to $t' \approx 0.7$. We also analyze the long-range behavior of the pair-pair correlation functions. We do not find obvious enhancement of pairing for the range of t' studied. The phase diagram based on DMRG results are shown in Fig. 1(c).

The ground state of the t' -Hubbard model on square lattice is found to be very sensitive to the boundary conditions and widths of the studied systems, indicating the presence of large finite-size effect [17]. To evaluate the finite-size effect in the width-4 systems studied, we compare the results with periodic (PBC) and antiperiodic (APBC) boundary conditions. The spin, charge, and pairing properties turn out to be insensitive to the boundary conditions in the half-filled stripe and AF Néel phases, indicating the results we obtained in this paper are likely to be representative of true two-dimensional systems.

II. MODEL AND METHOD

The Hamiltonian of the Hubbard model is

$$\hat{H} = - \sum_{(i,j),\sigma} t_{ij} (\hat{c}_{i\sigma}^\dagger \hat{c}_{j\sigma} + \text{H.c.}) + U \sum_i \hat{n}_{i\uparrow} \hat{n}_{i\downarrow} \quad (1)$$

where $\hat{c}_{i\sigma}^\dagger$ ($\hat{c}_{i\sigma}$) creates (annihilates) an electron on site $i = (x_i, y_i)$ with spin σ , and U represents the on-site Coulomb interaction. We consider electron hopping terms up to next-nearest neighbors (t') and set the nearest-neighbor hopping t as energy unit. We focus on $U = 8$ in this paper. We scan a range of t' from -0.7 to 0.7 . We only study the hole-doped case. The electron-doped case can be transformed to the hole-doped case by reversing the sign of t' through a particle-hole transformation. The averaged hole concentration away from half-filling is defined as $\delta = N_h/N$ with $N_h = \sum_i (1 - n_i)$. An illustration of the honeycomb lattice is sketched in Fig. 1(a). We rearrange it into a square lattice as shown in Fig. 1(b) to index the sites more conveniently. After the rearrangement, we study the square system with cylinder geometry, i.e., with periodic/antiperiodic (open) boundary conditions along y (x) direction. There are totally $N = L_x \times L_y$ lattice sites. We compare the results with PBC and APBC in our calculations to test the finite-size effect.

We employ DMRG [25,26] in this paper, which can provide accurate results of narrow cylinders [27,28]. We focus on $1/16$ hole-doping regime in which half-filled stripe was found in the model without t' before [13,14]. We calculate systems with width $L_y = 4$ and length $L_x = 32$. We apply AF pinning fields with strength $h_m = 0.5$ on the open edges of the width-4 cylinder, which allows us to detect spin order by measuring the local magnetization $\langle \hat{S}_i^z \rangle$ instead of the more demanding spin-spin correlation functions and makes the DMRG calculations easier to converge [30]. To characterize the charge and spin order, we define rung charge density as $n(x) = \sum_{y=1}^{L_y} \langle \hat{n}_i(x, y) \rangle / L_y$ along the width direction of the cylinders and staggered spin density as $(-1)^y \langle \hat{S}_i^z \rangle$. We also measure the singlet pair-pair correlation function defined as $D(r) = \langle \hat{\Delta}_i^\dagger \hat{\Delta}_{i+r} \rangle$ with $\hat{\Delta}_i^\dagger = \hat{c}_{(i,1),\uparrow}^\dagger \hat{c}_{(i,2),\downarrow}^\dagger - \hat{c}_{(i,1),\downarrow}^\dagger \hat{c}_{(i,2),\uparrow}^\dagger$. The state kept in the DMRG calculation is as large as $m = 11\,000$ with a typical truncation error $\epsilon \approx 1.5 \times 10^{-5}$ and careful extrapolations of DMRG results with truncation errors are performed in the converged region.

III. CHARGE AND SPIN DENSITIES

In Fig. 2, we show the results for charge and staggered spin-density profiles for various values of t' under PBC (upper

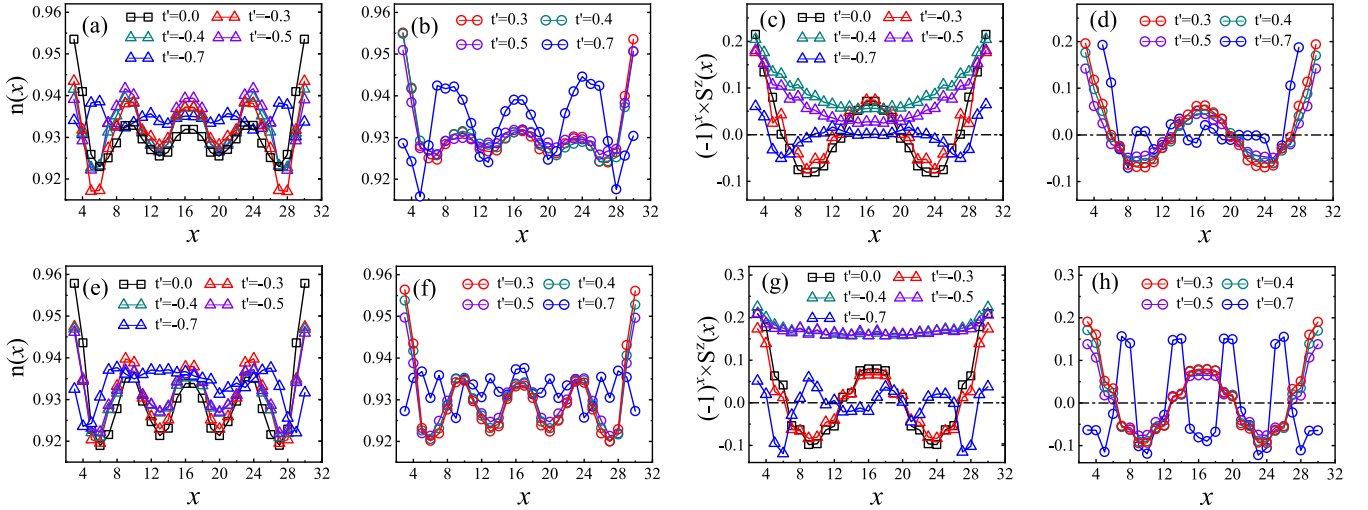


FIG. 2. Electron density and staggered spin density for positive [(b),(d)] and negative [(a),(c)] t' under PBC (upper panel) and APBC (lower panel). The dashed horizontal lines in (c), (d), (g), and (h) represent zero. We can find a phase transition from half-filled stripe order to AF Néel order at critical t'_c between -0.3 and -0.4 . The results for spin and charge density agree qualitatively between PBC and APBC in the half-filled stripe and AF Néel phases. The results are from extrapolation of truncation errors in DMRG except the ± 0.7 case and t' close to the phase transition point, for which results for largest bond dimension is shown. See the Supplemental Material [18] for details.

panel) and APBC (lower panel). As mentioned above, we only study the hole-doped cases and the electron-doped case can be mapped to the hole-doped case by reversing the sign of t' with a particle-hole transformation.

As shown in Figs. 2(b) and 2(f), in the positive t' side, when t' is small, the charge distribution $n(x)$ displays an oscillation with period $\lambda_\rho = 1/2\delta = 8$. And the spatial modulation of staggered spin density has a wavelength twice that of the charge density with a π phase flip at the hole concentrated sites [see Figs. 2(d) and 2(h)]. The spin and charge modulations are consistent with the half-filled stripe state found in the $t' = 0$ case [13,14] [also shown in Fig. 2(a)]. The half-filled stripe phase terminates at about $t' = 0.7$. When $t' \geq 0.7$, there is large discrepancy for the states obtained for PBC and APBC. The characterization of the phase in this region needs further investigation on wider systems.

In the negative t' side, the half-filled stripe phase at $t' = 0$ stretches to $t'_c \approx -0.3$, beyond which a phase transition occurs. When $t' < t'_c$, the system switches to an AF Néel phase with charge modulation as shown in Figs. 2(a), 2(e), 2(c), and 2(g). The charge-modulated Néel phase terminates at about $t' = -0.7$, beyond which the ground state is paramagnetic with nearly uniform density.

The results for spin and charge densities agree (quantitative difference still exists) with PBC and APBC in the half-filled stripe and AF Néel phases, suggesting the results are likely to be representative for the true two-dimensional system.

A phase diagram based on these results can be found in Fig. 1(c).

IV. PAIRING CORRELATION

The singlet pair-pair correlation function $D(r)$ is shown in Fig. 3 for a series of t' values. We plot the absolute value of $D(r)$ for A, B, and C bonds (see Fig. 1 for the definitions) under PBC and APBC in the upper and lower panes, respec-

tively. The reference bond is the C bond placed between sites (8, 2) and (9, 3) [see Fig. 1(b)]. We find that the long-distance behaviors of pair-pair correlation do not change qualitatively within the range of t' . They do not change qualitatively either under different boundary conditions. There is a tiny oscillation in the decay of the pair-pair correlations induced by the charge modulation.

On the square lattice, long-range pairing order emerges with the inclusion of t' [17]. But as shown in Fig. 3, we do not find obvious enhancement of pairing for the range of t' studied. Near the transition point $-0.4 < t' < -0.3$ where half-filled stripe switches to AF Néel order with charge modulation, the strength of $D(r)$ is actually slightly suppressed. We have also calculated the spin-triplet pair-pair correlations (see the results in the Supplement Material [18]) but found they are much weaker than the singlet pair-pair correlations.

In Fig. 4 we show the relative strengths of the pair-pair correlation for PBC and APBC with different t' values, by dividing the correlation on A and B bonds with the value on C bonds, which are connected by the same site. In the stripe phase (i.e., $|t'| < |t'_c|$), we can find that the relative strength of pair-pair correlations on A bonds is nearly equal to C bonds in magnitude but with opposite sign. And the pair-pair correlations on B bonds are very tiny comparing to the values on C bonds. Therefore, the pairing order have an approximate $(-1, 0, 1)$ sign structure locally, which is one of the degenerate d -wave representations d_{xy} of $D6h$ symmetry of the honeycomb lattice [31]. In the AF Néel phase [$t' = -0.5$ results in Figs. 4(d) and 4(h)], we can not find a clear pattern for the relative strength of the pairing correlations, which could be resulted from the finite-size effect.

V. SUMMARY AND PERSPECTIVES

We systematically study the evolution of the half-filled stripe order with next-nearest-neighbor hopping t' on the

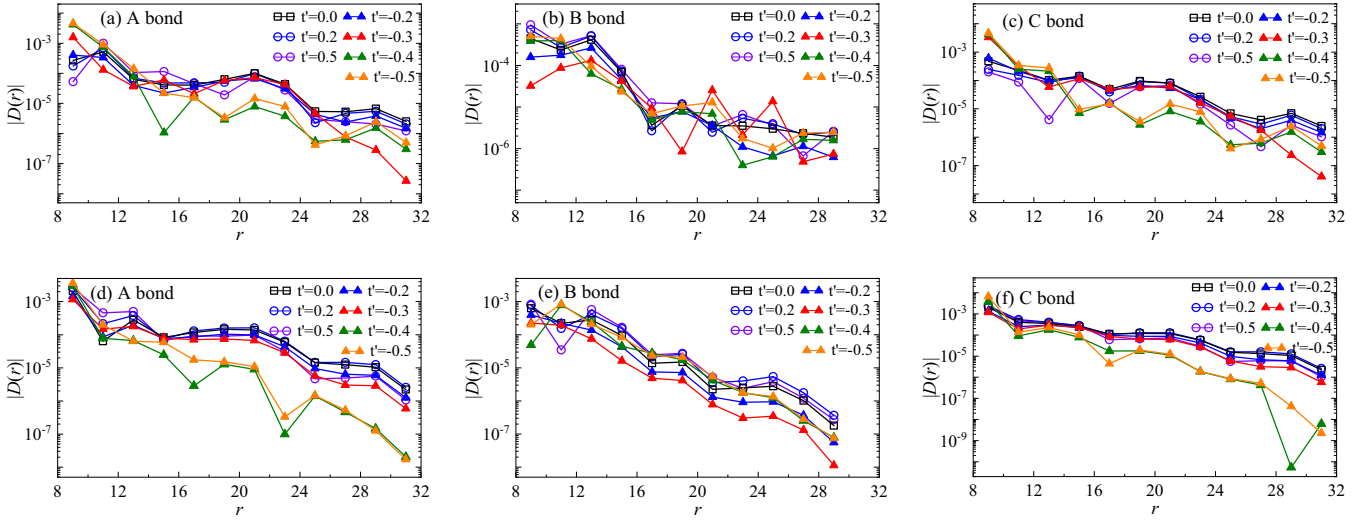


FIG. 3. Absolute value of pair-pair correlation functions of A [(a),(d)], B [(b),(e)], and C [(c),(f)] bonds for different t' . The upper (lower) panel denotes results with PBC (APBC). The reference bond is placed at the bond between site (8, 2) and (9, 3) to remove the boundary effect [29]. Notice that r is measured from the reference bond along the x direction in unit of the lattice constant. The long-distance behaviors of pair-pair correlation do not change qualitatively within the range of t' studied and under different boundary conditions.

slightly doped Hubbard model on honeycomb lattice in the strongly interacting region. We employ DMRG and study width-4 cylinders. In the negative t' side, the half-filled stripe phase is stable against the frustration of t' until a critical point $-0.4 < t'_c < -0.3$, at which a phase transition from half-filled stripe to AF Néel phase with charge modulation occurs. The charge-modulated AF Néel phase terminates at about $t' = -0.7$. In the positive t' side, the half-filled stripe state stretches to about $t' = 0.7$. Different from the square lattice case [17], we do not find obvious enhancement of pairing for the range of t' studied. The results with PBC and

APBC agree qualitatively in the half-filled stripe and AF Néel phases, indicating the results in this work are likely to be representative for real two-dimensional system. Experimentally, long-range AF Néel order was observed in Na_2IrO_3 [32] and $\text{InCu}_{2/3}\text{V}_{1/3}\text{O}_3$ [33] in which the contributions are from the $1/2$ spin on a honeycomb lattice. Moreover, Hubbard model on honeycomb lattice was also realized on cold atom platform [34]. It will be interesting to see the realization of the phases and phase transitions found in this paper in real materials or in ultracold atom platforms in the future.

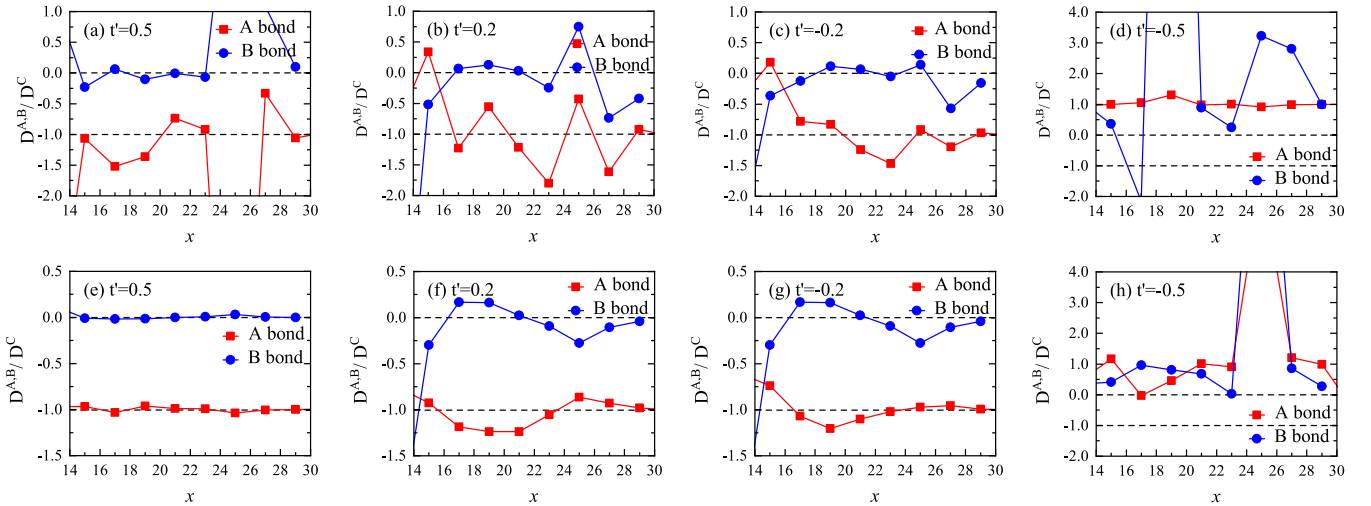


FIG. 4. The relative strengths of the pair-pair correlations for bonds connected by the same site. The relative strength is defined by dividing the correlation on A and B bonds with the value on C bonds, which are connected by the same site, i.e., D^A/D^C and D^B/D^C . The upper (lower) panel denotes results under PBC (APBC) with different t' . The reference bond is placed at the bond between sites (8, 2) and (9, 3). The dashed horizontal lines represent 0 and -1 . In the half-filled stripe phase [(a)–(c) and (e)–(g)], we can find a $(-1, 0, 1)$ sign structure at long distance, which is the d_{xy} representation of the $D6h$ symmetry of the honeycomb lattice. In the AF Néel phase [(d) and (h)], we can not find a clear pattern for the relative strength of the pairing correlations.

ACKNOWLEDGMENTS

Y.S. and M.P.Q. thank Weidong Luo for his generosity to provide computational resources for this work. M.P.Q. acknowledges the support from the National Key Research and Development Program of MOST of China

(Grant No. 2022YFA1405400), the National Natural Science Foundation of China (Grant No. 12274290), the Innovation Program for Quantum Science and Technology (Grant No. 2021ZD0301900) and the sponsorship from Yangyang Development Fund.

-
- [1] P. A. Lee, N. Nagaosa, and X.-G. Wen, *Rev. Mod. Phys.* **78**, 17 (2006).
- [2] J. Hubbard, *Proc. R. Soc. Lond. A* **276**, 238 (1963).
- [3] D. J. Scalapino, *Rev. Mod. Phys.* **84**, 1383 (2012).
- [4] M. Qin, T. Schäfer, S. Andergassen, P. Corboz, and E. Gull, *Annu. Rev. Condens. Matter Phys.* **13**, 275 (2022).
- [5] D. P. Arovas, E. Berg, S. A. Kivelson, and S. Raghu, *Annu. Rev. Condens. Matter Phys.* **13**, 239 (2022).
- [6] J. P. F. LeBlanc, A. E. Antipov, F. Becca, I. W. Bulik, G. K.-L. Chan, C.-M. Chung, Y. Deng, M. Ferrero, T. M. Henderson, C. A. Jiménez-Hoyos *et al.* (Simons Collaboration on the Many-Electron Problem), *Phys. Rev. X* **5**, 041041 (2015).
- [7] B.-X. Zheng, C.-M. Chung, P. Corboz, G. Ehlers, M.-P. Qin, R. M. Noack, H. Shi, S. R. White, S. Zhang, and G. K.-L. Chan, *Science* **358**, 1155 (2017).
- [8] M. Qin, C.-M. Chung, H. Shi, E. Vitali, C. Hubig, U. Schollwöck, S. R. White, and S. Zhang (Simons Collaboration on the Many-Electron Problem), *Phys. Rev. X* **10**, 031016 (2020).
- [9] A. H. Castro Neto, F. Guinea, N. M. R. Peres, K. S. Novoselov, and A. K. Geim, *Rev. Mod. Phys.* **81**, 109 (2009).
- [10] Y. Otsuka, S. Yunoki, and S. Sorella, *Phys. Rev. X* **6**, 011029 (2016).
- [11] F. F. Assaad and I. F. Herbut, *Phys. Rev. X* **3**, 031010 (2013).
- [12] S. Sorella and E. Tosatti, *Europhys. Lett.* **19**, 699 (1992).
- [13] X. Yang, H. Zheng, and M. Qin, *Phys. Rev. B* **103**, 155110 (2021).
- [14] M. Qin, *Phys. Rev. B* **105**, 035111 (2022).
- [15] Z.-T. Xu, Z.-C. Gu, and S. Yang, *Phys. Rev. B* **108**, 035144 (2023).
- [16] C. Peng, D. Sheng, and H.-C. Jiang, [arXiv:2303.12348](https://arxiv.org/abs/2303.12348).
- [17] H. Xu, C.-M. Chung, M. Qin, U. Schollwöck, S. R. White, and S. Zhang, [arXiv:2303.08376](https://arxiv.org/abs/2303.08376).
- [18] See Supplemental Material at <http://link.aps.org/supplemental/10.1103/PhysRevB.109.024505> for physical quantities with finite bond dimension and the extrapolation results for different t' 's. The evolution of the noninteracting dispersion on the honeycomb lattice with t' is also displayed.
- [19] F. Ferrari, S. Bieri, and F. Becca, *Phys. Rev. B* **96**, 104401 (2017).
- [20] S.-S. Gong, D. N. Sheng, O. I. Motrunich, and M. P. A. Fisher, *Phys. Rev. B* **88**, 165138 (2013).
- [21] F. Mezzacapo and M. Boninsegni, *Phys. Rev. B* **85**, 060402(R) (2012).
- [22] R. F. Bishop, P. H. Y. Li, D. J. J. Farnell, and C. E. Campbell, *J. Phys.: Condens. Matter* **24**, 236002 (2012).
- [23] J. Reuther, D. A. Abanin, and R. Thomale, *Phys. Rev. B* **84**, 014417 (2011).
- [24] B. K. Clark, D. A. Abanin, and S. L. Sondhi, *Phys. Rev. Lett.* **107**, 087204 (2011).
- [25] S. R. White, *Phys. Rev. Lett.* **69**, 2863 (1992).
- [26] S. R. White, *Phys. Rev. B* **48**, 10345 (1993).
- [27] U. Schollwöck, *Rev. Mod. Phys.* **77**, 259 (2005).
- [28] E. Stoudenmire and S. R. White, *Annu. Rev. Condens. Matter Phys.* **3**, 111 (2012).
- [29] Y. Shen, G.-M. Zhang, and M. Qin, *Phys. Rev. B* **108**, 165113 (2023).
- [30] S. R. White and A. L. Chernyshev, *Phys. Rev. Lett.* **99**, 127004 (2007).
- [31] A. M. Black-Schaffer and S. Doniach, *Phys. Rev. B* **75**, 134512 (2007).
- [32] Y. Singh and P. Gegenwart, *Phys. Rev. B* **82**, 064412 (2010).
- [33] V. Kataev, A. Möller, U. Löw, W. Jung, N. Schittner, M. Kriener, and A. Freimuth, *J. Magn. Magn. Mater.* **290-291**, 310 (2005).
- [34] T. Uehlinger, G. Jotzu, M. Messer, D. Greif, W. Hofstetter, U. Bissbort, and T. Esslinger, *Phys. Rev. Lett.* **111**, 185307 (2013).